



1 **More dynamic than expected: An updated survey of surging glaciers** 2 **in the Pamir**

3 Franz Goerlich¹, Tobias Bolch², Frank Paul¹

4 ¹Department of Geography, University of Zurich, Zurich, Switzerland

5 ²School of Geography and Sustainable Development, University of St. Andrews, St. Andrews, United Kingdom

6 *Correspondence to:* Franz Goerlich (franz.goerlich@geo.uzh.ch)

7 **Abstract.** The investigation of surging glaciers using remote sensing has recently seen a strong increase as freely
8 available satellite data and digital elevation models (DEMs) can provide detailed information about surges that
9 often take place in remote or inaccessible regions. Apart from analysing individual surges, satellite information is
10 increasingly used to collect capable data on surging glaciers. Related inventories have recently been published for
11 several regions in High Mountain Asia including the Karakoram, parts of the Pamir and western Kunlun Shan,
12 but information for the entire Pamir is solely available from a historic database listing about 80 glaciers with
13 confirmed surges. Here we present an updated inventory of confirmed glacier surges for the Pamir that considers
14 results from earlier studies and is based on a systematic analysis of Landsat image time series (1988 to 2018) and
15 DEM differences. Actively surging glaciers were identified from animations, flicker images and the typical
16 elevation change patterns. Selected historic and contemporary very high-resolution imagery were used to confirm
17 surges. In total, we identified 206 spatially distinct surges within 186 glacier bodies, mostly clustered in the
18 northern and central part of the Pamir. Where possible, minimum and maximum glacier extents were digitized,
19 but often interacting tributaries made a clear separation challenging. Most surging glaciers (n=70) are found in
20 the larger size classes (>10 km²), but two of them are very small (<0.5 km²). We found also several surges where
21 the length of the glacier increased by more than 100%. The created datasets are available at:
22 <https://doi.pangaea.de/10.1594/PANGAEA.914150> (Goerlich et al., 2020).

23

24 **1 Introduction**

25 The investigation of surging glaciers using satellite data received recently increased attention among scientists, in
26 particular for the Karakoram mountain range but also other regions of the world (Berthier and Brun, 2019;
27 Bhambri et al., 2017; Bolch et al., 2017; Falaschi et al., 2018; Minora et al., 2016; Paul, 2015; Quincey et al.,
28 2015; Rankl and Braun, 2016; Round et al., 2017; Steiner et al., 2018). This has several reasons, for example (a)
29 the free access to long (Landsat) and dense (TerraSAR-X / TanDEM-X, Sentinel-1/2) time series of high-
30 resolution satellite data, (b) the limited understanding of why some glaciers in this region are surging while
31 others do not, (c) a high amount of on-going surges at any point in time, (d) the large variations of surge
32 behaviour in a small region, (e) the long history and still occurring surge-related hazards (mostly due to damming
33 of a river and related outburst of lakes), and (f) the very difficult field access. Thereby, most of the studies
34 document the variations in glacier extent / length changes, flow velocities and elevation / mass changes in the



35 course of a surge or surge-related hazards. These studies revealed unprecedented details about surge dynamics
36 and variations that already helped in improving our understanding of related surge mechanisms.

37

38 In contrast, the surging glaciers in the Pamir mountain ranges to the north of the Karakoram received less
39 attention, but recently some studies were published (e.g. Lv et al. 2019; Osipova 2015; Wendt et al. 2017; Holzer
40 et al. 2016). This might be due to the fact that several surges during the Soviet era have already been described in
41 detail (e.g. the surges of Medvezhy and Geographical Society glaciers are well documented, see Dolgushin and
42 Osipova (1971, 1975), Kotlyakov et al. (2003) and Osipova (2015) and a detailed inventory describing a high
43 number (>800) of surge-type glaciers based on satellite data and aerial images was published (Osipova et al.
44 1998). However, this and many of the publications are in Russian and are therefore little known internationally.

45

46 When speaking about surging glaciers, we first have to differentiate between surge-type glaciers and other
47 glaciers. This is important when interpreting glacier changes in the context of climate change, e.g. their length or
48 mass changes over a time period where surges have occurred (Bolch et al., 2017; Brun et al., 2017; Gardelle et
49 al., 2013). Secondly, it is also important to distinguish surge-type from surging glaciers. The former have surged
50 at some point in the past and show indirect evidences (e.g. looped or distorted moraines, post-surge down-
51 wasting features) of a former surge, whereas the latter surged actively within the observation period. We here
52 only investigate the latter. The globally most complete compilation of surge-type glaciers by Sevestre and Benn
53 (2015) is a most valuable starting point but is based on literature sources up to the year 2013 only. In the
54 meantime, numerous further surge-type glaciers have been identified across High Mountain Asia (HMA) from
55 the analysis of multi-temporal satellite imagery, e.g. in the Karakoram (Bhambri et al., 2017), Kunlun Shan
56 (Yasuda and Furuya, 2015), central Tibet (Zhang et al., 2018), eastern Pamir (Lv et al., 2019) and Tian Shan
57 (Mukherjee et al., 2017), but an update of confirmed surges for the entire Pamir Mountains is yet missing. With
58 this study we aim at identifying them and providing detailed information (e.g. timing and typology) about
59 confirmed surges in the Pamir Mountains.

60

61 Surge-type glaciers are included in the inventory by Osipova et al. (1998) and Sevestre and Benn (2015). The
62 information from the former study is also available in the Randolph Glacier Inventory (RGI) version 6 (RGI
63 Consortium 2017) using the simplified classification scheme developed by the latter study (with three instead of
64 six classes). We have revisited existing literature, the RGI and the new study by Lv et al. (2019) as a starting
65 point for our inventory of confirmed glacier surges. It is primarily based on the analysis of animated multi-
66 temporal (1988-2018) time-series of Landsat data, but also on elevation difference maps showing the typical
67 mass transfer pattern of glacier surges. For some less clear cases, we also analysed very high-resolution images
68 from the Corona and Hexagon missions and the maps in Google Earth and bing.com for confirmation.

69

70 There are thus important differences in our approach compared to the methodology used for the ‘catalogue’ by
71 Osipova et al. (1998), implying that both are not directly comparable: (i) our satellite image time series (Landsat
72 has a lower spatial resolution (30 m) than the KFA1000 data (3-5 m) used by Osipova et al. (1998), (Dowdeswell
73 et al. 1993, 1995), (ii) we cover a different period (1988–2018) than Osipova (1998), have (iii) used different



74 indicators for surge identification (e.g. animations, DEM difference patterns), (iv) assigned only one surge class
75 instead of six. and (v) our glacier entities have different boundaries as we used the most recent inventory by Mölg
76 et al. (2018) as a base for the analysis.

77
78 For this study, we revisited this inventory (here named GI-1) by adding ice divides for glacier units that surged
79 but were so far connected with other glaciers in GI-1, resulting in a new inventory GI-2. In a second step, three
80 inventory subsets are created that provide (a) the selection of surging glaciers only from the GI-2 inventory (GI-
81 3), (b) minimum (GI-3min), and (c) maximum (GI-3max) extents of all surging glaciers. The number in brackets
82 after a glaciers name refers to its ID in the GI-3min inventory. We also present a rough classification of the
83 different surge-types, the timing of surges during the observation period (1988-2018), a comparison of
84 geomorphometric characteristics (other glaciers in GI-2 vs. GI-3), and an analysis of the geometric changes (e.g.
85 minimum elevation) due to a surge.

86 **2 Study region**

87 The Pamir is one of highest mountain ranges within HMA and of the world extending from about 36°35' to
88 39°35' N and 70°35' to 75°35' E (Fig. 1). The northern part belongs to the Osh region of Kyrgyzstan, the eastern
89 parts to the Xinjiang Uighur Autonomous Region of China, the most southern regions to Badakhshan in
90 northeastern Afghanistan and the main part to Gorno-Badakhshan in Tajikistan. The highest peak (Mt. Kongur)
91 reaches up to 7649 m a.s.l. and enthrones over the Kongur Shan in the eastern part of the Pamir (all names are
92 based on selected transliterated Russian topographic maps at a 1:500.000 and 1:100.000 scale).

93

94 *Figure 1*

95

96 Typical glaciers in the Pamir are long and dendritic or multi-basin valley glaciers, but other types such as
97 mountain glaciers and cirques exist as well. Due to the steep and ice-free surrounding rock walls, most glaciers
98 are at least partly debris covered, which simplifies the identification of typical surge marks (e.g. looped moraines)
99 from space (e.g. Kotlyakov et al. 2008). Most glaciers are concentrated in the central part around Ismoil Somoni
100 Peak (7495 m a.s.l.) including Fedchenko Glacier, which is with a length of >70 km the longest valley glacier in
101 the world outside the polar regions (Machguth and Huss, 2014). Additionally, the region is home of abundant
102 rock glaciers that are not always clearly separable from debris-covered glaciers and other ice-debris landforms
103 (Mölg et al., 2018).

104

105 The glaciers in the western and central part of the Pamir (Tadjik, Kyrgyz and Afghan regions) are of winter
106 accumulation type where most precipitation (~90%) falls between December and May (Maussion et al., 2014)
107 with annual amounts of up to 1285 mm a⁻¹ at Fedchenko weather station (Finaev et al., 2016). Contrary, the
108 glaciers in the eastern part are mainly (50 to 60%) fed by precipitation in the summer months between June and
109 August, which can be seen as an outpost of the monsoon (Maussion et al., 2014). The total annual precipitation is
110 very low in some regions, reaching only ~70 mm a⁻¹ at Murgab (3576 m a.s.l.) and Toxkargan weather stations,
111 both located in valleys (3090 m a.s.l.) (Finaev et al., 2016). Hence, the glaciers in the western and central part are



112 situated in a somewhat warmer and more humid climate whereas the eastern ranges are dry and cold.
113 Accordingly, mean elevations of the former can be found at lower altitudes (~4740 m a.s.l.) than in the eastern
114 regions (~5050 m a.s.l.) (Mölg et al., 2018).

115

116 The likely best-investigated glacier in the region is Fedchenko (Lambrecht et al., 2014, 2018) that is so far
117 considered as not surging. Of the glaciers with confirmed surges, Medvezhy Glacier (29) is likely the best
118 investigated (see Kotlyakov et al., 2008). This latter study is also reporting details about surges of several other
119 glaciers in the region, partly back to 1959.

120 **3 Datasets and pre-processing**

121 **3.1 Satellite data**

122 **3.1.1 Landsat**

123 For the detection of glacier surges and determination of surge start, end and possibly cycle, we used freely
124 available Landsat imagery (Level 1T) from earthexplorer.usgs.gov including Landsat 5 TM (Thematic Mapper),
125 Landsat 7 ETM+ (Enhanced Thematic Mapper plus) and Landsat 8 OLI (Operational Land Imager) sensors.
126 Additionally, we used some very good scenes (no snow outside glaciers) from Landsat MSS (Multispectral
127 Scanner) from the 1970s and 1980s. The three sensors TM, ETM+ and OLI acquire data with a horizontal
128 resolution of 30 m for the visible, near-infrared (NIR) and shortwave infrared (SWIR) bands at a repeat rate of 16
129 days. Key characteristics of the datasets are shown in Table 1, the full list of scenes used for this study is
130 presented in Table S1 in the Supplementary material.

131

132 In general, cloud-free scenes from the end of the summer (July to October) are used from all sensors, but for
133 some regions, also earlier acquisitions are considered to have images available for as many years as possible.
134 With a focus on the changes near the glacier terminus, the remaining seasonal snow at higher elevations in these
135 images was unproblematic. Unfortunately, it was not possible to find suitable scenes for each year in most
136 regions so that the determination of the onset or end of a surge has at least a ± 1 year uncertainty. Priority was
137 given to Landsat 5 TM scenes to limit using Landsat 7 ETM+ scenes after 2002 when the Scan Line Corrector
138 (SLC) stopped working (resulting in so-called SLC-off scenes). For the animations we use the standard colour-
139 balanced and orthorectified image quicklooks that are provided in false-colours (glacier ice and snow is depicted
140 in cyan) at the original resolution and were downloaded from earthexplorer.usgs.gov. The jpg-compression of
141 these images results locally in blurred details but they had only very small impact on surge identification.

142

143 *Table 1*

144

145 **3.1.2 Corona and Hexagon**

146 The Corona Keyhole (KH) 4B scenes from August 1968 (Table S1) cover the central and northern Pamir (see
147 Fig. 1) and were also downloaded from earthexplorer.usgs.gov. The Corona images are panchromatic, recorded



148 in stereo mode and have a ground resolution of up to 1.8 m (Galiatsatos, 2009). We processed 11 scene pairs to
149 generate a DEM and corresponding orthophotos with 5 m resolution following Goerlich et al. (2017). Due to the
150 high effort of processing Corona stereo scenes, the orthoimages cover the region with the most surging glaciers.
151 The orthoimages revealed details in surface morphology that are typical for surging glaciers but barely visible for
152 the largest glaciers at the 30 or 15 m resolution of Landsat images. We also used Hexagon KH-9 scenes from July
153 1975 and June 1980 to generate orthoimages following Pieczonka et al. (2013). The scenes depict the regions
154 west of Fedchenko Glacier up to a resolution of 6 m.

155 3.1.3 Google Earth and bing.com

156 The very high-resolution satellite images available in Google Earth (GE) have been widely used for numerous
157 geoscientific applications (Liang et al., 2018). We used them here together with the satellite images available on
158 bing.com to confirm identified surging glaciers in the Landsat period, i.e. for visual checks only. Sometimes the
159 available time series in GE also allowed a proper identification of glacier surges when the quiescent and/or active
160 phases are captured (see examples in Lv et al., 2019). Interestingly, the images used in bing.com were often
161 complimentary to GE, i.e. provided excellent coverage when nothing useful was available in GE and vice versa.
162

163 In Fig. 2 we provide a visual comparison of image sources displaying three surging glaciers in the central Pamir
164 to illustrate the visibility of details. We include examples from Corona, Hexagon, Landsat OLI as well as geo-eye
165 (from bing.com). The high-resolution images from Corona and bing.com show clearly the highly crevassed
166 surfaces (mainly for the two larger glaciers) that are not visible in the Landsat image. In the Landsat image, the
167 glacier boundary and debris-covered parts can be identified, but it is almost impossible to reveal the terminus of
168 Walter 731 (19) and Soldatov (20) glaciers in the static image. This is different when using animations that reveal
169 glacier termini clearly when they change position (Paul, 2015).

170

171 *Figure 2*

172

173 3.2 Digital elevation models (DEMs)

174 Several DEMs are freely available for the study region. This includes the Shuttle Radar Topography Mission
175 (SRTM) DEM (Rabus et al., 2003), the Advanced Spaceborne Thermal Emission and Reflection Radiometer
176 (ASTER) GDEMv2 (Tachikawa et al., 2011), the ALOS PRISM DEM AW3D30 (Takaku et al., 2014), the High
177 Mountain Asia (HMA) DEM (Shean, 2017) and the DEM from the TanDEM-X mission (TDX) provided by DLR
178 (German Aerospace Centre) (Wessel, 2016). They have different characteristics (sensor types, spatial resolution,
179 artefacts, data voids, acquisition dates) and – apart from the HMA DEM – are used here for several purposes such
180 as calculation of topographic characteristics and surface elevation changes (Table 2). A direct comparison of the
181 DEMs using hillshades and DEM differences revealed that only the GDEMv2 and the AW3D30 DEM are free of
182 data voids but that the GDEMv2 has partly strong artefacts over glacier surfaces. We thus used the AW3D30
183 DEM to determine topographic characteristics for all glaciers.

184



185 Besides the orthoimages, we created DEMs from the 1968 Corona stereo pairs (cf. Goerlich et al., 2017) and used
186 DEMs from 1975 Hexagon data (cf. Pieczonka et al., 2013). The AW3D30 DEM served as a height reference
187 (Ground Control Points, Disparity Predictions) for the Corona DEM processing and the SRTM DEM for
188 Hexagon. The main difference of the final DEMs is the coverage where Corona covers only a small area (~15 x
189 180 km²) per stereo image pair compared to Hexagon (~130 x 130 km²). This results in a far larger effort to
190 generate DEMs and orthophotos from Corona for a larger region.

191

192 We have used the temporarily better constrained DEMs from Corona (1968), SRTM (2000), AW3D30 (2006-
193 2011), and TDX (2011-2014) to determine elevation changes over the periods of 1968 to 2000, 2000 to ~2009,
194 and ~2009 to ~2012/14. Elevation differences were interpreted in a qualitative sense only as the typical pattern of
195 elevation changes for surging glaciers (strong elevation gain/loss in the lower and vice versa in their upper region
196 during the active/quiescent phase of a surge) can be clearly identified in most cases, i.e. changes are often much
197 higher (100+ m) than the combined uncertainties of the two DEMs (e.g. Gardelle et al. 2013).

198

199 *Table 2*

200

201 **3.3 Glacier outline datasets**

202 We used the Karakoram / Pamir glacier inventory (GI-1) created by Mölg et al. (2018) as a basis for glacier
203 identification and extent modification. This inventory provides a consistent dataset of manually corrected glacier
204 outlines based on Landsat scenes acquired between 1998 and 2002 for the entire Pamir, including the ranges
205 Kingtau, Ulugarttag and Muztagh in the Chinese part. As the inventory is a temporal snap shot and surge-type
206 glaciers are in various stages of their surge cycle, they can be connected to a larger main glacier and thus not be
207 analysed separately. To overcome this restriction, we have separated all part-time tributaries exhibiting their own
208 dynamics from the glaciers they connect with and added the required new ice divides in the accumulation
209 regions. This revised inventory (GI-2) is used as the base for all subsequent geomorphometric calculations. The
210 separation follows the natural flow and extent of the larger glacier and required several iterations, as the surge
211 characteristic was often not clear from the beginning. After all surges have been identified, a sub-sample of GI-2
212 was created that only includes the glaciers that surged (inventory GI-3). The GI-3 sub-sample served as a base to
213 digitise minimum and maximum glacier extents for all glaciers exhibiting a visible change in terminus position.
214 These datasets are saved in two additional inventories (GI-3min and GI-3max, respectively).

215 **4. Methods**

216 **4.1 Surge identification**

217 Glacier surges can occur in very different forms and flavours with a likely continuous transition to instable flow
218 and regular glacier advances. Hence, a clear identification of surge-type glaciers is not trivial even in their active
219 phase and a wide range of identification criteria has been suggested to distinguish them from all other glaciers
220 (e.g. Sevestre et al., 2015; Bhambri et al., 2017; Mukherjee et al., 2017). In this study, we focus on glaciers that



221 had an active surge phase during the investigated period 1988-2018, i.e. indirect evidences alone such as distorted
222 or looped moraines are not considered. In consequence, our sample is smaller than the one presented in the
223 ‘catalogue’ by Osipova et al. (1998), who listed 845 surge-type glaciers for the Pamir (i.e. 35% of the global
224 sample by Sevestre and Benn (2015)) in six distinct classes. Their inventory is also digitally available in the RGI
225 using the simplified classification scheme by Sevestre and Benn (2015), with the classes (their Table 4):
226 confirmed (Category 1), probable (2) and possible (3). With our focus on observed surges (with few exceptions)
227 our sample would be in the ‘confirmed’ type of which Osipova et al. (1998) list 61 and Sevestre and Benn (2015)
228 90 glaciers.

229

230 To identify surging glaciers, we started with the ‘confirmed’ samples listed by Osipova et al. (1998, 2010),
231 Kotlyakov et al. (2008) and Lv et al. (2019). These studies included all mountain ranges where we searched for
232 surging glaciers except the Rushanskii and Muztagh ranges. Our identification consists of four steps:

233

234 (I) At first, we analysed the animations from the Landsat quicklooks to validate the findings of the four studies.
235 Each frame set was animated with slightly different samples to facilitate visibility of glacier dynamics in each
236 region similar to Paul (2015). The qualitative analysis tracked surface feature displacements and was applied to
237 the entire study region. Collectively, this step revealed 139 surging glaciers during the study period (including
238 glaciers that have just started surging).

239 (II) In the next step, we analysed the elevation change patterns of the various DEM difference maps in a
240 qualitative way (Mukherjee et al., 2017). Glaciers showing an opposing pattern of surface elevation change
241 (lowering and thickening) were digitally marked and added to the sample, yielding 35 further glaciers from the
242 1968 to 2000 and 2000 to c. 2009 elevation difference maps. An example of the DEM difference map is
243 displayed in Fig. 3, revealing for some glaciers the typical surge pattern. This method helped in detecting internal
244 surges with limited changes of the terminus and/or where crevasses or shear margins are difficult to detect.

245

246 *Figure 3*

247

248 (III) In this step, we analysed individual image pairs in detail using flicker images, i.e. going back and forth
249 between two images only (Kääb et al. 2003). For a clear before/after distinction, this analysis was restricted to the
250 best scenes available for a specific region (e.g. without clouds, seasonal snow or deep shadows). We here also
251 used the contrast-enhanced false colour infrared images from the MSS scenes, several 15 m panchromatic images
252 of ETM+ and OLI and the declassified orthoimages. Additional 27 glaciers could be identified this way.

253

254 (IV) In the final step, we checked the identified glaciers with the partially very high-resolution images available
255 in GE and bing.com to also analyse morphological characteristics of the glacier surfaces in detail, their shape and
256 also possible changes in extent (Lv et al., 2019). Despite the variability in acquisition years, this allowed us
257 removing a few glaciers (7) from the sample (in most cases the ‘surges’ were likely just advances) and also
258 adding 12 new ones. At this stage, we started introducing indirect evidence to the classification and thus checked



259 back if the (mostly small) glaciers have really surged using animations. In some cases it was necessary to
260 interpret results from steps (I) to (III) collectively for a reasonable result.

261

262 Based on the created inventory subset with surging glaciers only (GI-3), we digitised the minimum (GI-3min)
263 and maximum (GI-3max) extent of all glaciers based on the satellite images described in Section 3.1. For glaciers
264 with more than one surge, the respective largest and smallest extents were digitised (Fig. 4). Whereas maximum
265 extents are in most cases well identifiable, outlines for GI-3min can have larger uncertainties due to the
266 difficulties in clearly identifying the new terminus among the often debris-covered and down-wasting ice from
267 the previous surge. Ideally, the minimum extent is identified once the next surge started, but for many glaciers
268 this did not happen during the observation period.

269

270 *Figure 4*

271

272 **4.2 Surge characteristics and classification**

273 There is a wide range of possibilities to characterise surges as they have a high variability of appearance and
274 dynamics (e.g. Bhambri et al. 2017). For the GI-3min inventory we have determined a series of key surge
275 characteristics in the attribute table (e.g. surge start / end / duration, and distance) and a simplified classification
276 according to a pre-defined criteria set for statistical analysis and comparison with other regions. It has to be noted
277 that a precise start/end year was often difficult to determine either due to missing satellite data, but also when
278 surge initiation is related to a mass wave coming down from higher elevations (taking a few years) or when
279 remaining dead ice from a previous surge was reactivated. We here defined the start of a surge as the year when
280 an advance of the terminus or a mass wave higher up the glacier (as not all surges show a terminus advance) is
281 detectable. The end of the active phase (maximum extent) is reached when all surge dynamics settle and the
282 quiescent phase begins. This was easier to determine than minimum extents in most cases.

283

284 To illustrate a few of the possible surge types and interactions, Fig. 5 displays a sketch map of three glaciers that
285 are all surging at some stage. Starting with a surge of the permanently connected tributary (2) in Fig. 5a, this
286 surge is at its maximum extent in Fig. 5b and the ice from the surge is already slightly moved downstream by the
287 flow of the main glacier (1). In addition, glacier (3) started surging in the meantime, connects to the main glacier
288 in Fig. 5b and enters glacier (1) in Fig. 5c where it also reaches its maximum extent. Some time later (Fig. 5d),
289 also the main glacier (1) is in full surge mode and transports the surge marks of both tributary surges
290 downstream, stretching and possibly deforming them. This should illustrate the variety of surge interactions (by
291 far not all) and the difficulty to define maximum extents of tributary glaciers. Their surge marks are moved
292 downstream by the main glacier during or near the end of their own surge due to its normal flow or its own surge.
293 Accordingly, there is also some uncertainty in the timing of the surge end for glaciers (2) and (3). In this case the
294 main glacier body would have listed 2 surges in the attribute table of GI-3min and has been selected to receive
295 the classification code.

296



297 *Figure 5*

298

299 For the classification scheme, we used the following criteria and values for each glacier:

300 (A) ‘surging?’: no 0, yes 1, if yes:

301 (B) glacier tongue: free end 1, connects to another glacier 2, tributary 3

302 (C) type of surge: advancing 1, internal 2, combined 3

303 (D) active phase duration: 1-3 years 1, 4-10 years 2, >10 years 3

304 (E) terminus advance: none 0, short (<1 km) 1, medium (1-2.5 km) 2, long (> 2.5 km) 3.

305 Hence, the entry in the attribute table of GI-2 is either 0 or 1 and stored in a separate ‘surge’ column. The
306 resulting code from our classification in GI-3min is then for example 2123. This means that the glacier is
307 connected to another glacier during its surge, that it has an advancing tongue and surged over a period of 4-10
308 years over a medium distance. In the case the glacier already surged in 1988 or was still surging in 2018, these
309 two years were used as the start or end date. Such dates indicate that the real surge duration is likely longer than
310 given in the table.

311 **4.3 Topographic and other information**

312 For all glaciers in GI-2, we calculated the following attributes: centre point latitude and longitude, area in km²,
313 minimum, maximum, mean, and median elevation, mean slope and aspect, and aspect sector. All attributes are
314 also transferred to GI-3, and additionally calculated for GI-3min and GI-3max.

315 **5. Results**

316 **5.1 Distribution and topographic characteristics of surge and other glaciers**

317 From the ~13500 glaciers in the study region, 186 have been separated as surging glaciers of which 206 spatially
318 distinct surges have been identified between 1988 and 2018. Their occurrence is clustered in the central, northern
319 (central and western Pamir Alai, Fedchenko and ‘Petr Alervogo East’) and eastern ranges (Muztagh and
320 Ulugarttag) (Fig. 6). This pat-tern leaves a large gap for glacier surges in the central Pamir (around lake Karakul)
321 and to the south of the study region with few exceptions. Overall, the latter regions are dominated by comparably
322 smaller glaciers and drier climate, indicating that there might be a size and climatic threshold for surge activity as
323 suggested by Sevestre and Benn (2015).

324

325 *Figure 6*

326

327 The 186 surging glaciers cover a total area of ~2670 km² (with ~110 km² variability due to the surges). About
328 5% of them are smaller than 1 km² covering an area of ~7 km², whereas 38% are larger than 10 km² covering an
329 area of 2170 km² (or 81%) (Table 3). The largest non-surging glacier, Fedchenko, is a huge dendritic valley
330 glacier with a size of ~580 km² (without the Bivachny tributary) and is covering 6% of the total glacier area. The
331 region is thus dominated by the vast size of Fedchenko Glacier with impacts on size-related distributions. Eight



332 surging glaciers are smaller than 1 km² at their minimum extent (the smallest has a size of 0.3 km²) and the
333 largest surging glacier is the Garmo Glacier main trunk (80) with a minimum extent of ~83 km².

334

335 *Table 3*

336 The created inventories have a different count of entries due to different glacier states and topologic relations.
337 The generalised statistics for the sample with observed surges refer to the GI-3 inventory with 186 entries whilst
338 statistics for GI-3min and GI-3max have different numbers. Compared to the full sample of glaciers in GI-2
339 (13495), surging glaciers constitute 77% by number and 80% by area in the area class 50-100 km² (Fig. 7). They
340 are also dominating the size classes 10-50 and 100-500 km² (51% and 63% by area, respectively). When
341 considering all three size classes from 10 to 500 km², two thirds of the glaciers are surging, i.e. they are the rule
342 rather than the exception. The 22 largest surging glaciers cover almost the same area (1338 km²) than the 163
343 smaller ones (1332 km²).

344

345 *Figure 7*

346

347 The mean aspect sector distribution of surge glaciers is only slightly different from all other glaciers (Fig. 8a).
348 Surging glaciers exposed to SW contribute almost 14% to the sample whereas only 3% of the other glaciers are
349 facing in this direction. The same applies to the area covered (Fig. 8b), where surging glaciers cumulate ~370
350 km² and thus ¼ more area than the other glaciers (~300 km²) in this sector. On the other hand, the latter have
351 higher percentages facing NW, N and NE. The strong difference towards the NE is due to Fedchenko Glacier.

352

353 *Figure 8*

354

355 The scatter plot showing mean elevation vs. mean aspect (Fig. 9) reveals that mean elevations cover a wide range
356 of values (from about 3500 to 6000 m) and that there is some dependence on aspect, i.e. glaciers facing south
357 have a few hundred metres higher mean elevations. The surging glaciers largely follow the distribution, but have
358 somewhat higher elevations in the southern and lower values in the northern aspect ranges compared to the other
359 glaciers when considering mean values per sector. On average, their mean elevation is 4800 m a.s.l.

360

361 *Figure 9*

362

363 Median glacier elevations increase from west to east and show a small decrease in the most eastern and northern
364 ranges (Pamir Alai) towards the outer glaciers (Fig. 10). The marked surging glaciers are mostly found along the
365 outer boundary of the study region with generally lower median elevations. The near absence of surging glaciers
366 in the inner Pamir with its generally higher median elevations is noteworthy. However, in the Mustagh region,
367 glaciers with observed surges have the highest (5646 m) and surging glaciers in the 'Petr Alervogo west' region
368 the lowest values (3429 m).

369



370 *Figure 10*

371

372 As surging glaciers have a bias towards larger sizes compared to all other glaciers (see Fig. 7), they also have
373 slightly higher elevation ranges (Fig. 11a) and form the upper end of the sample. However, the spread of values
374 for glaciers with a size of about 50 km² is very large, ranging from about 2000 to nearly 5000 m. The area-
375 elevation distribution in Fig. 11b displays a smaller amount of area around the mean elevation compared to all
376 other glaciers, which is likely due to the many small glaciers in these altitudes (see black circles in Fig. 10).

377

378 *Figure 11*

379

380 **5.2 Observed changes**

381 For a sample of 169 and 160 glaciers, we could map their minimum and maximum extent, respectively and for
382 148 surges determine the surge duration. For 15 glaciers, we observed a full surge cycle with the onset of the next
383 surge and for six glaciers (Bivachny 63, Dzerzhinsky 104, Medvezhy 29, Right Dustiroz 31, Yazgulemdara 35, 1)
384 two or more surges were observed over the study period. Both, the timing of the surges and their durations are
385 highly variable (Fig. 12). Moreover, one has to consider that several glaciers (>30) were already surging on the
386 first available Landsat TM images (in 1988) and several (>20) are still surging in 2017/2018. For both cases the
387 surge duration could not be fully determined and is thus longer than the here presented values.

388

389 *Figure 12*

390

391 The two histograms in Fig. 13 display a counting of the surges that started in a particular period (Fig. 13a) and of
392 the surge durations in 4-year bins (Fig. 13b). For both graphs it has to be considered that the first period
393 (1988/89) is including all glaciers that are already surging at that time. This gives a much higher number of
394 surges (66) compared to those that have only started in 1989 (27). For the surge duration counting in Fig. 13b this
395 means that shorter surge periods are over-represented and are indeed longer. Furthermore, the last period is not
396 complete (i.e. surges are on-going), which has the same effect on the counting. This results in possibly too high
397 and too low values in the first and last period, respectively. To circumvent this problem, we have also counted all
398 surges that took place fully within the period, i.e. started in 1989 or later and ending in 2017 or before (black bars
399 in Fig. 13b). This sample is much smaller but has still a reasonable amount of glaciers in all classes. Figure 13a
400 reveals that the number of surges that have started in the second and third period is the same and slowly declining
401 afterwards. The surge duration counting displayed in Fig. 13b has a peak at 1-5 years and very similar numbers
402 for the next four intervals. Only few glaciers (9) have surge durations exceeding 21 years.

403

404 *Figure 13*

405

406 The simplified typology counting presented in Table 4 is revealing that 75% of all glaciers have freely advancing
407 tongues, whereas 18% connect to another glacier at least in their maximum extent. From the total sample of



408 identified surging glaciers, 85% (176 glaciers) are considerably advancing whereas the remaining 15% (26) are
409 surging internally with none or only a minor terminus advance. The latter were sometimes hard to detect and
410 required application of additional measures (see Section 3). From the glaciers with a substantial terminus
411 advance, most (49%) advance up to 1 km. Larger advances of up to 2.5 km are found for 27% of the glaciers and
412 8.5% advanced more than 2.5 km (up to 6.7 km). Most of the advancing glaciers are situated in the central
413 mountain ranges around Fedchenko Glacier, whereas the eastern ranges are dominated by stable glaciers and
414 internal surges (but with a high variability). The strongest advance has Garmo Glacier (80) in the Garmo
415 mountain range with 6665 m.

416

417 *Table 4*

418

419 One of the most active glaciers is Medvezhy Glacier (29) with a surge cycle of only ~10 years and an active
420 period of just 2 years (Kotlyakov et al., 2018). Further glaciers with relatively short (≤ 5 years) active phases are
421 spread all over the study region. During the active surge phase, 128 glaciers increased their area by a total of
422 ~119 km², which is 6% of their total area (GI-3min) and 4% of the total area in the GI-2 inventory. On average,
423 the minimum elevation decreased from 3953 m a.s.l. to 3789 m a.s.l., but individual glaciers are reaching up to
424 ~1300 m further down at their maximum extent. The change in minimum elevation due to a surge does not
425 depend on the elevation range (or size) of the glacier. This is also related to the fact that several large glaciers
426 show mostly internal surges with maybe only a small advance of the tongue. On the other hand, several smaller
427 glaciers with a comparably small elevation range (less than 1000 m) increase their elevation range by a factor of
428 two and more. Similarly, also length changes due to a surge do not depend on glacier size or length. However, it
429 is noteworthy that some glaciers change their length by about a factor of two or even more. The two most
430 extreme glaciers are just 1.8 and 1.9 km long and surge over a distance of ~ 3.5 km.

431 **6. Discussion**

432 **6.1 Characteristics of the surging glaciers and their surges**

433 Surging glaciers dominate the area classes above 10 km², which would confirm earlier observations that surging
434 glaciers are comparably large (Barrand and Murray, 2006; Clarke et al., 1986; Mukherjee et al., 2017). However,
435 we found that they can also be smaller than 1 km², down to 0.3 km². Why such small glaciers surge, often
436 increasing their length considerably, needs to be further investigated. We also have to mention that there might be
437 even smaller glaciers that were not detected due to the coarse resolution of the satellite data, i.e. our sample is
438 somewhat biased towards larger glaciers. Whereas the aspect distribution of surging glaciers is very similar to all
439 other glaciers (Fig. 8), they seem to have lower median elevations than other glaciers when facing north and
440 higher ones when facing south (Fig. 9). We do not have a physical explanation for this and assume it might only
441 be an artefact of the sampling. Their spatial distribution, on the other hand, is more peculiar as they are mostly
442 found in the outer regions of the study site (Figs. 5 and 10). Their higher share of large elevation ranges (Fig.
443 11a) is related to their generally larger size and their hypsometry is very similar to other glaciers.

444



445 Within the period considered here, the starting dates of surges are comparably random (Fig. 12), indicating a
446 limited impact of climatic trends on the timing. Surge durations (11 years in the mean) are as diverse as in the
447 Karakoram (Bhambri et al., 2017; Paul, 2020). However, complete surge cycles are not observed for many
448 glaciers (from one start of an active phase to the next), so this impression is biased by the observation window.
449 Due to gaps in satellite data availability, we might have missed a few glaciers displaying only (short) internal
450 surges, so the real number of surging glaciers might be even higher and the number of glaciers with a short
451 duration of active phases higher than in our sample.

452 **6.2 Criteria to identify surges**

453 The criteria we applied to identify surges were handled flexible to consider the wide range of surge types found
454 in the region. However, the differentiation between surging and ‘only’ advancing glaciers is sometimes
455 challenging and other interpretations are possible. The very high-resolution images as available for our study site
456 from Corona / Hexagon and Google Earth / bing.com did not help much in determining the timing of a surge (due
457 to the large temporal gaps), but were most helpful in confirming the surge nature of a glacier in previous and
458 recent times, respectively (Lv et al. 2019, Paul 2020). The historic images clearly reveal that many glaciers in the
459 Pamir Mountains have also surged in the 1970s, however we have not used them here to derive the timing of
460 these earlier surges as this would be a large additional exercise and the temporal density of available images
461 might not be sufficient. However, we used them to confirm additional minimum and maximum extents.

462 **6.3 Uncertainties**

463 Regarding the uncertainties of the derived topographic characteristics, one has to consider that we used the GI-1
464 basis inventory from around 2000 with a DEM (AW3D30) from around 2009 (Takaku et al., 2014). The DEM
465 has local artefacts and the timing of both datasets does not match. The latter is in particular the case for glaciers
466 that surged between 2000 and 2009 and had strong changes in geometry. The strongest impact is likely on
467 minimum elevation and glacier length, but also median elevation, aspect and mean slope are impacted. There is
468 little we can do about this uncertainty, as otherwise we would need a DEM from nearly every year, synchronous
469 with the timing of the minimum glacier extent. However, for the overall statistical analysis of the datasets
470 presented here, the impact of the temporal mismatch on the graphs is likely small. Of course, when individual
471 glaciers are analysed, this mismatch has to be considered (Frey and Paul, 2012).

472

473 Regarding the timing of the observed surges, we face the following uncertainties:

- 474 a) We have only analysed the time window 1988 to 2018; the assigned duration of surges starting before 1988 or
475 ending after 2018 is thus too short,
- 476 b) we only include glaciers with an active surge phase between 1988 and 2018; the real number of surging
477 glaciers in the study region might thus be higher,
- 478 c) for most regions we do not have usable satellite images in every year (e.g. due to snow and clouds); this adds
479 to the uncertainty of the start/end assignment and could even result in completely missed short-lived internal
480 surges,



481 d) the spatial resolution of Landsat sometimes impact on a proper identification of the terminus, in particular
482 when debris-covered; this leads to uncertainties in the timing,
483 e) due to residual dead ice in the glacier forefield and debris cover, the timing of the minimum extent is more
484 difficult to define than the maximum; in uncertain cases we used the extent from GI-3, and
485 f) when surges start with a mass wave and/or stay internal (no terminus advance), the timing derived from visual
486 analysis will likely be different from studies analysing flow velocities.
487 Collectively, it is likely that other analysts derive different start/end dates of a surge, but in most cases the
488 difference will not exceed a few years. This will thus not affect the overall conclusions about the highly variable
489 timing of surges and surge durations.

490

491 The here presented assignment of surge classes should be robust as we basically used qualitative and categorised
492 criteria that will not change much for a different interpretation. However, not all surges of the same glacier end
493 up in the same class. For example, if a recent surge is more dynamic than a previous one, it might reach another
494 glacier and become a part-time tributary. Also internal surges might have shown advancing termini before and
495 are thus not strictly internal. Hence, the assigned classes can vary for other surges.

496 **6.4 Comparison to other inventories**

497 Compared to previous studies, we identified several new surging glaciers. Some of the probable or possible
498 (category 2 and 3) surges listed in Osipova et al. (1998) have indeed surged and are now included in our
499 inventory. Most others found in these categories could not be confirmed as the morphological details used to
500 identify surge activities are only visible in very high-resolution imagery (at least 2 m) rather than with 30 or 15 m
501 Landsat data we used here. Of course, it is well possible that they surged outside our observation window.

502

503 Sevestre and Benn (2015) presented 561 possible surge-type glaciers in the Pamir based on the inventory by
504 Osipova et al. (1998). Our findings are in good agreement with the 51 most reliably classified (3) surge-type
505 glaciers marked in the RGI (we include 45 of them). Our 132 additional surging glaciers belong mostly (55 of
506 188) to category (2) in the RGI, and a few (18 of 322) belong to category (1). The remaining 52 surging glaciers
507 were not indicated as surge-type in the RGI. Outlines from two of our surging glaciers (65 and 64) are missing in
508 the RGI 6.0.

509

510 Compared to Lv et al. (2019), we identified three further surging glaciers (16 in total) in the King Tau and
511 Ulugarttag sub-regions. Apart from surge-type glaciers, their study also classified four glaciers as advancing,
512 eleven as stable and one retreating. We classified one of their advancing and three of their stable glaciers as
513 surging. This new interpretation results from our longer observation period and the DEM difference images
514 revealing the typical mass redistribution patterns. The surging glaciers described by Kotlyakov et al. (2008) is in
515 full agreement with our findings. The above-mentioned numbers have to be handled with care as we had to
516 compare two different inventories with individual glacier divides. Thus, a direct and one-to-one comparison is
517 challenging.



518 **7. Conclusions**

519 In this study, we presented a new inventory of surging glaciers for the Pamir Mountains. The analysis is based on
520 results from earlier studies, Landsat imagery acquired over the period 1988 to 2018, the SRTM and ALOS DEM
521 and declassified very-high resolution images from Corona and Hexagon. Using animations and flicker images for
522 the Landsat time series in combination with the elevation change patterns from DEM differencing, we detected
523 206 spatially distinct glacier surges within 186 glacier bodies. The new dataset is in good agreement with
524 previous compilations of surging glaciers and confirmed surges for 133 new glaciers that were so far only marked
525 as surge-type probable or possible. We further digitized minimum and maximum extent of 169 and 160 glaciers,
526 respectively, and determined the timing for about $\frac{3}{4}$ of all surges. The temporal distribution is random in regard
527 to timing and surge duration (mean value 11 years). The distribution of surging glaciers is biased towards the
528 central, northern and eastern mountain ranges. Their sizes range from 0.3 to 143 km² and they are dominating the
529 size-class distribution above 10 km². Several glaciers descend by more than 800 m (one glacier) or increased their
530 length by a factor of more than 2 (5) during a surge. However, advance distances are not related to original
531 glacier length as several large glaciers only show internal surges or very small advances. The three inventories
532 created in this study (GI-3, GI-3min/max) are available to serve as a base for further investigations.

533 **8. Data availability**

534 The dataset can be downloaded from: <https://doi.pangaea.de/10.1594/PANGAEA.914150> (Goerlich et al., 2020).

535 **Author contribution**

536 F.G. and F.P. designed the study, analysed the datasets and wrote the manuscript, F.G. processed the data and
537 prepared all figures and datasets. T.B. provided additional literature and datasets and contributed to the writing
538 and editing of the manuscript.

539 **Competing interests**

540 The authors declare that they have no conflict of interest.

541 **Acknowledgements**

542 The work of F.G. and F.P. was supported by the ESA projects Glaciers_cci (4000109873/14/I-NB) and
543 Glaciers_cci+ (4000127593/19/I-NB), the work of T.B. was partially supported by the Strategic Priority Research
544 Program of Chinese Academy of Sciences (XDA20100300). The AW3D30 DEM is provided by the Japan
545 Aerospace Exploration Agency (<http://www.eorc.jaxa.jp/ALOS/en/aw3d30/index.htm>) ©JAXA. All Corona,
546 Hexagon and Landsat images used in this study were provided by USGS and downloaded from
547 earthexplorer.usgs.gov. We thank P. Rastner for supporting us in calculating the topographic parameters for
548 several states of the inventory, K. Mukherjee for providing the Hexagon DEMs from 1975 and H. Machguth for
549 providing the centre lines for determination of glacier length and length changes.



550 References

- 551 Barrand, N. E. and Murray, T.: Multivariate Controls on the Incidence of Glacier Surging in the Karakoram
552 Himalaya, Arctic, Antarct. Alp. Res., 38(4), 489–498, doi:10.1657/1523-
553 0430(2006)38[489:MCOTIO]2.0.CO;2, 2006.
- 554 Berthier, E. and Brun, F.: Karakoram geodetic glacier mass balances between 2008 and 2016: Persistence of the
555 anomaly and influence of a large rock avalanche on Siachen Glacier, *J. Glaciol.*, 65(251), 494–507,
556 doi:10.1017/jog.2019.32, 2019.
- 557 Bhambri, R., Hewitt, K., Kawishwar, P. and Pratap, B.: Surge-type and surge-modified glaciers in the
558 Karakoram, *Sci. Rep.*, 7(15391), 1–14, doi:10.1038/s41598-017-15473-8, 2017.
- 559 Bolch, T., Pieczonka, T., Mukherjee, K. and Shea, J.: Brief communication: Glaciers in the Hunza catchment
560 (Karakoram) have been nearly in balance since the 1970s, *Cryosphere*, 11(1), 531–539, doi:10.5194/tc-11-
561 531-2017, 2017.
- 562 Brun, F., Berthier, E., Wagnon, P., Kääb, A. and Treichler, D.: A spatially resolved estimate of High Mountain
563 Asia glacier mass balances from 2000 to 2016, *Nat. Geosci.*, 10(9), 668–673, doi:10.1038/ngeo2999, 2017.
- 564 Clarke, K. C., Sciamoi, P., Simon, C. and Ommanney, L.: Characteristics of Surge-Type Glaciers, *J. Geophys.*
565 *Res.*, 91(5), 7165–7180, doi:10.1029/JB091iB07p07165, 1986.
- 566 Dolgushin, L. D. and Osipova, G. B.: New Data on the recent Glacier Surges, *Mater. Glyatsiol.*, 18, 191–217,
567 1971.
- 568 Dolgushin, L. D. and Osipova, G. B.: Glacier surges and the problem of their forecasting, *IAHS Publ.* (104),
569 292–304, 1975.
- 570 Dowdeswell, J. A., Gorman, M. R., Macheret, Y. Y., Moskalevsky, M. Y. and Hagen, J. O.: Digital comparison
571 of high resolution Sojuzkarta KFA-1000 imagery of ice masses with Landsat and SPOT data, *Ann. Glaciol.*,
572 17, 105–112, doi:10.3189/S0260305500012684, 1993.
- 573 Dowdeswell, J. A., Glazovsky, A. F. and Macheret, Y. Y.: Ice divides and drainage basins on the ice caps of
574 Franz Josef Land, Russian High Arctic, defined from Landsat, KFA-1000, and ERS-1 SAR satellite imagery,
575 *Artic Alp. Res.*, 27(3), 264–270, doi:10.1080/00040851.1995.12003121, 1995.
- 576 Falaschi, D., Bolch, T., Lenzano, M. G., Tadono, T., Lo Vecchio, A. and Lenzano, L.: New evidence of glacier
577 surges in the Central Andes of Argentina and Chile, *Prog. Phys. Geogr.*, 42(6), 792–825,
578 doi:10.1177/0309133318803014, 2018.
- 579 Finaev, A. F., Shiyin, L., Weijia, B. and Li, J.: Climate Change And Water Potential Of The Pamir Mountains, in
580 *Geography, Environment, Sustainability*, pp. 88–105., 2016.
- 581 Frey, H. and Paul, F.: On the suitability of the SRTM DEM and ASTER GDEM for the compilation of:
582 Topographic parameters in glacier inventories, *Int. J. Appl. Earth Obs. Geoinf.*, 18(1), 480–490,
583 doi:10.1016/j.jag.2011.09.020, 2012.
- 584 Galiatsatos, N.: The Shift from Film to Digital Product: Focus on CORONA Imagery, *Photogramm. -*
585 *Fernerkundung - Geoinf.*, 2009(3), 251–260, doi:10.1127/0935-1221/2009/0020, 2009.
- 586 Gardelle, J., Berthier, E., Arnaud, Y. and Kääb, A.: Region-wide glacier mass balances over the Pamir-
587 Karakoram-Himalaya during 1999-2011, *Cryosphere*, 7(4), 1263–1286, doi:10.5194/tc-7-1263-2013, 2013.
- 588 Goerlich, F., Bolch, T., Mukherjee, K. and Pieczonka, T.: Glacier Mass Loss during the 1960s and 1970s in the
589 Ak-Shirak Range (Kyrgyzstan) from Multiple Stereoscopic Corona and Hexagon Imagery, *Remote Sens.*,
590 9(275), doi:10.3390/rs9030275, 2017.
- 591 Goerlich, F., Bolch, T., Paul, F.: Inventory of surging glaciers in the Pamir. PANGAEA,
592 <https://doi.pangaea.de/10.1594/PANGAEA.914150>, 2020.
- 593 Holzer, N., Gollez, T., Buchroithner, M. F. and Bolch, T.: Glacier Variations in the Trans Alai Massif and the
594 Lake Karakul Catchment (Northeastern Pamir) Measured from Space, in R.P. Singh, U. Schikhoff, & S. Mal
595 (Eds.): *Climate Change, Glacier Response, and Vegetation Dynamics in the Himalaya*, edited by R. P. Singh,
596 U. Schikhoff, and S. Mal, pp. 139–153, Springer, Cham., 2016.
- 597 Kääb, A., Isakowski, Y., Paul, F., Neumann, A. and Winter, R.: Glaziale und periglaziale Prozesse: Von der
598 statischen zur dynamischen Visualisierung, *Kartographische Nachrichten*, 53(5), 206–212, 2003.
- 599 Kotlyakov, V. M., Desinov, L. V., Osipova, G. B., Hauser, M., Tsvetkov, D. G. and Schneider, J. F.: Events in
600 2002 on Russian Geographical Society (RGO) Glacier, Pamirs, *Mater. Glyatsiol.*, 95, 221–230, 2003.
- 601 Kotlyakov, V. M., Osipova, G. B. and Tsvetkov, D. G.: Monitoring of the Pamirs surging glaciers from space,
602 *Ann. Glaciol.*, 48, 125–134, doi:10.3189/172756408784700608, 2008.
- 603 Kotlyakov, V. M., Chernova, L. P., Khromova, T. E., Muraviev, A. Y., Kachalin, A. B. and Tiufliin, A. S.:
604 Unique Surges of Medvezhy Glacier, *Dokl. Earth Sci.*, 483(2), 1547–1552, doi:10.1134/s1028334x18120152,
605 2018.
- 606 Lambrecht, A., Mayer, C., Aizen, V., Floricioiu, D. and Surazakov, A.: The evolution of Fedchenko glacier in the



- 607 Pamir, Tajikistan, during the past eight decades, *J. Glaciol.*, 60(220), 233–244, doi:10.3189/2014JoG13J110,
608 2014.
- 609 Lambrecht, A., Mayer, C., Wendt, A., Floricioiu, D. and Völksen, C.: Elevation change of Fedchenko Glacier,
610 Pamir Mountains, from GNSS field measurements and TanDEM-X elevation models, with a focus on the
611 upper glacier, *J. Glaciol.*, 64(246), 637–648, doi:10.1017/jog.2018.52, 2018.
- 612 Liang, L., Cuo, L. and Liu, Q.: The energy and mass balance of a continental glacier: Dongkemadi Glacier in
613 central Tibetan Plateau, *Sci. Rep.*, 8(1), 1–8, doi:10.1038/s41598-018-31228-5, 2018.
- 614 Lv, M., Guo, H., Lu, X., Liu, G., Yan, S., Ruan, Z., Ding, Y. and Quincey, D. J.: Characterizing the behaviour of
615 surge- and non-surge-type glaciers in the Kingata Mountains, eastern Pamir, from 1999 to 2016, *Cryosphere*,
616 13(1), 219–236, doi:10.5194/tc-13-219-2019, 2019.
- 617 Machguth, H. and Huss, M.: The length of the world’s glaciers a new approach for the global calculation of
618 center lines, *Cryosphere*, 8(5), 1741–1755, doi:10.5194/tc-8-1741-2014, 2014.
- 619 Maussion, F., Scherer, D., Mölg, T., Collier, E., Curio, J. and Finkelnburg, R.: Precipitation seasonality and
620 variability over the Tibetan Plateau as resolved by the high Asia reanalysis, *J. Clim.*, 27(5), 1910–1927,
621 doi:10.1175/JCLI-D-13-00282.1, 2014.
- 622 Minora, U., Bocchiola, D., D’Agata, C., Maragno, D., Mayer, C., Lambrecht, A., Vuillermoz, E., Senese, A.,
623 Compostella, C., Smiraglia, C. and Diolaiuti, G. A.: Glacier area stability in the Central Karakoram National
624 Park (Pakistan) in 2001–2010: The “Karakoram Anomaly” in the spotlight., 2016.
- 625 Mölg, N., Bolch, T., Rastner, P., Strozzi, T. and Paul, F.: A consistent glacier inventory for Karakoram and Pamir
626 derived from Landsat data: Distribution of debris cover and mapping challenges, *Earth Syst. Sci. Data*, 10(4),
627 1807–1827, doi:10.5194/essd-10-1807-2018, 2018.
- 628 Mukherjee, K., Bolch, T., Goerlich, F., Kutuzov, S., Osmonov, A., Pieczonka, T. and Shesterova, I.: Surge-type
629 glaciers in the Tien Shan (Central Asia), Arctic, Antarct. Alp. Res., 49(1), 147–171,
630 doi:10.1657/AAAR0016-021, 2017.
- 631 Osipova, G. B.: Fifty years of studying the Medvezhiy Glacier (West Pamirs) by the Institute of Geography,
632 RAS, *Ice Snow*, 1, 129–140, doi:10.15356/2076-6734-2015-1-129-140, 2015.
- 633 Osipova, G. B. and Khromova, T. E.: Electronic data base “Surging glaciers of Pamir,” *Ice Snow*, 4, 15–24, 2010.
- 634 Osipova, G. B., Tsvetkov, D. G., Schetinnikov, A. S. and Rudak, M. S.: Inventory of surging glaciers of the
635 Pamirs, *Mater. Glyatsiol.*, 85, 3–136, 1998.
- 636 Paul, F.: Revealing glacier flow and surge dynamics from animated satellite image sequences: Examples from the
637 Karakoram, *Cryosphere*, 9(6), 2201–2214, doi:10.5194/tc-9-2201-2015, 2015.
- 638 Paul, F.: A 60-year chronology of glacier surges in the central Karakoram from the analysis of satellite image
639 time-series, *Geomorphology*, 352, 106993, doi:10.1016/j.geomorph.2019.106993, 2020.
- 640 Pieczonka, T., Bolch, T. and Buchroithner, M.: Generation and evaluation of multitemporal digital terrain models
641 of the Mt. Everest area from different optical sensors, *ISPRS J. Photogramm. Remote Sens.*, 66(6), 927–940,
642 doi:10.1016/j.isprsjprs.2011.07.003, 2011.
- 643 Pieczonka, T., Bolch, T., Junfeng, W. and Shiyin, L.: Heterogeneous mass loss of glaciers in the Aksu-Tarim
644 Catchment (Central Tien Shan) revealed by 1976 KH-9 Hexagon and 2009 SPOT-5 stereo imagery, *Remote
645 Sens. Environ.*, 130, 233–244, doi:10.1016/j.rse.2012.11.020, 2013.
- 646 Quincey, D. J., Glasser, N. F., Cook, S. J. and Luckman, A.: Heterogeneity in Karakoram glacier surges, *J.
647 Geophys. Res. Earth Surf.*, 120(7), 1288–1300, doi:10.1002/2015JF003515, 2015.
- 648 Rabus, B., Eineder, M., Roth, A. and Bamler, R.: The shuttle radar topography mission—a new class of digital
649 elevation models acquired by spaceborne radar, *ISPRS J. Photogramm. Remote Sens.*, 57(4), 241–262,
650 doi:10.1016/S0924-2716(02)00124-7, 2003.
- 651 Rankl, M. and Braun, M.: Glacier elevation and mass changes over the central Karakoram region estimated from
652 TanDEM-X and SRTM/X-SAR digital elevation models, *Ann. Glaciol.*, 57(71), 273–281,
653 doi:10.3189/2016AoG71A024, 2016.
- 654 Round, V., Leinss, S., Huss, M., Haemmig, C. and Hajnsek, I.: Surge dynamics and lake outbursts of Kyagar
655 Glacier, Karakoram, *Cryosphere*, 11(2), 723–739, doi:10.5194/tc-11-723-2017, 2017.
- 656 Sevestre, H. and Benn, D. I.: Climatic and geometric controls on the global distribution of surge-type glaciers:
657 Implications for a unifying model of surging, *J. Glaciol.*, 61(228), 646–662, doi:10.3189/2015JoG14J136,
658 2015.
- 659 Shean, D.: High Mountain Asia 8-meter DEM Mosaics Derived from Optical Imagery, Version, Boulder,
660 Colorado., 2017.
- 661 Steiner, J. F., Kraaijenbrink, P. D. A., Jiduc, S. G. and Immerzeel, W. W.: Brief Communication : The Khurdopin
662 glacier surge revisited – extreme flow velocities and formation of a dammed lake in 2017, *Cryosph.*, 12(1),
663 95–101, 2018.
- 664 Tachikawa, T., Hato, M., Kaku, M. and Iwasaki, A.: Characteristics of ASTER GDEM version 2, Vancouver,
665 BC., 2011.



- 666 Takaku, J., Tadono, T. and Tsutsui, K.: Generation of high resolution global DSM from ALOS PRISM, *Int. Arch.*
667 *Photogramm. Remote Sens. Spat. Inf. Sci. - ISPRS Arch.*, 40(4), 243–248, doi:10.5194/isprsarchives-XL-4-
668 243-2014, 2014.
- 669 Wendt, A., Mayer, C., Lambrecht, A. and Floricioiu, D.: A Glacier Surge of Bivachny Glacier, Pamir Mountains,
670 Observed by a Time Series of High-Resolution Digital Elevation Models and Glacier Velocities, *Remote*
671 *Sens.*, 9(4), 388, doi:10.3390/rs9040388, 2017.
- 672 Wessel, B.: *TanDEM-X Ground Segment – DEM Products Specification Document*”, Oberpfaffenhofen. [online]
673 Available from: <https://tandemx-science.dlr.de/>, 2016.
- 674 Yasuda, T. and Furuya, M.: Dynamics of surge-type glaciers in West Kunlun Shan, Northwestern Tibet, *J.*
675 *Geophys. Res. F Earth Surf.*, 120(11), 2393–2405, doi:10.1002/2015JF003511, 2015.
- 676 Zhang, H., Zhang, F., Zhang, G., Ma, Y., Yang, K. and Ye, M.: Daily air temperature estimation on glacier
677 surfaces in the Tibetan Plateau using MODIS LST data, *J. Glaciol.*, 64(243), 132–147,
678 doi:10.1017/jog.2018.6, 2018.
- 679



680 **Tables**

681

682 *Table 1: Main characteristics of the satellite scenes used (see Table S1 for scene list).*

Satellite	Sensor	Resolution	Period	Purpose
Corona	KH-4	2-5 m	1968	DEM generation, high-res. info
Hexagon	KH-9	5-10 m	1975/1980	Additional DEM and high-res. info
Landsat	MSS	60 m	1972-1980	Extension back in time
Landsat	TM	30 m	1989-2012	Animation
Landsat	ETM+	30 m	1999-2018	Animation
Landsat	OLI	30 m	2013-2018	Animation

683

684

685 *Table 2: Selected characteristics of available DEMs and their usage in this study.*

DEM	Type	Sensor	Resolution	Acquisition period	Date of tiles?	Usage
GDEM2	optical	ASTER	30 m	1999-2015	No	Heights for Corona
SRTM	SAR-C	SRTM	30 m	Feb 2000	Yes	Elevation changes
ALOS	optical	PRISM	30 m	2007-2011	No	Topographic parameters, elevation changes 2000 to 2009
TDX	SAR-X	TanDEM-X	90 m	2012-2015	No	Elevation changes ~2009 to ~2014
Corona	optical	KH4-B	15 m	1968	Yes	Elevation changes 1968 to 2000; Orthophoto

686

687 *Table 3: Size class distribution of surge-type glaciers and other glaciers of GI-2 and GI-3.*

Size Class km ²		<0.05	0.05	0.1	0.5	1	5	10	50	100	>500
			-	-	-	-	-	-	-	-	
			0.1	0.5	1	5	10	50	100	500	
other glaciers	km ²	103.7	154.7	1104	1090.7	3353.4	1172.7	1190.1	167.8	154	580.3
	%	1.1	1.7	12.2	12	37	12.9	13.1	1.9	1.7	6.4
surge glaciers	km ²	0	0	0.4	6.1	174.2	319.7	1229	682.9	262.6	0
	%	0	0	0	0.2	6.5	12	46	25.5	9.8	0
all glaciers	km ²	103.7	154.7	1104.5	1096.9	3527.6	1492.3	2419.2	850.6	416.6	580.3
	%	0.9	1.3	9.4	9.3	30	12.7	20.6	7.2	3.5	4.9
Surge-type proportion in %		0	0	0	0	0	21.4	50.8	80.3	63	0

688

689

690 *Table 4: Results of the surge-type classification (counting per class). Glaciers without terminus advance (marked with a "0" for the duration criteria) are not listed here.*

691

DEM	1	2	3	Total
Tongue	150	32	16	198
Type	169	25	4	198
Duration	21	63	114	198
Distance	98	53	17	168

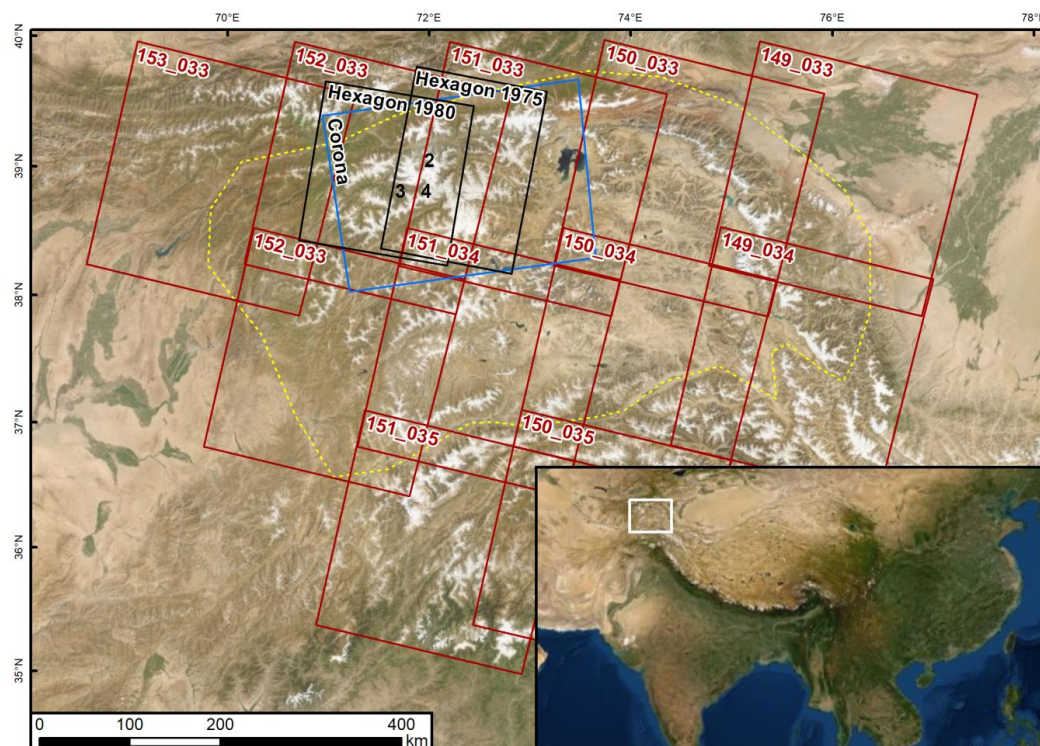
692

693



694 **Figures**

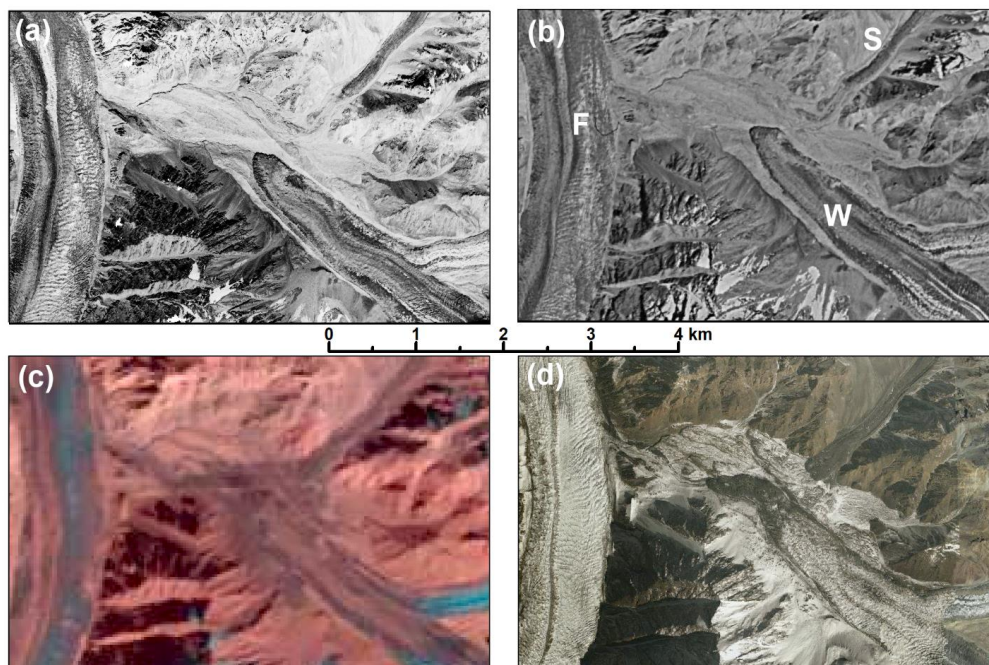
695



696

697 *Fig. 1: Location of the study region (white square in the inset) and footprints of the Corona (blue), Hexagon*
698 *(black) and Landsat (red) scenes used in this study. The dashed yellow line marks the perimeter of the study*
699 *region. The location of the sub-regions displayed in Figs. 2, 3 and 4 are marked with their respective numbers.*
700 *Image sources: screenshots from © Google Earth.*

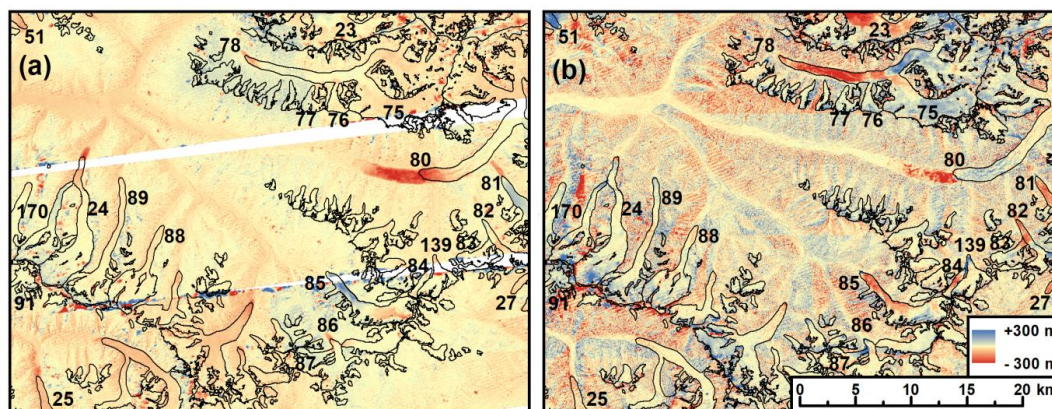
701



702

703 Fig. 2: Comparison of satellite images for the same sub-region (see Fig. 1 for location) showing the following
704 glaciers: F: Fortambek (18), W: Walter 731 (19), and S: Soldatov (20). The images are acquired by a) Corona in
705 1968, b) Hexagon in 1975, c) Landsat in 2017, and d) bing.com (date unknown). Image sources: Panels a) to c)
706 earthexplorer.usgs.gov, panel d) screenshot from bing.com ©2020 DigitalGlobe.

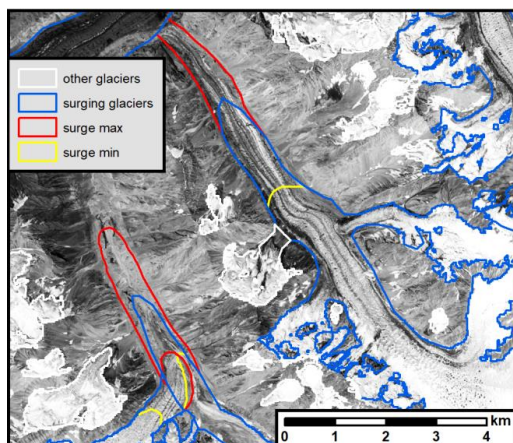
707



708

709 Fig. 3: Two examples of colour-coded DEM difference images used to identify surging glaciers (marked with
710 their ObjectID). A) SRTM-Corona and b) AW3D30-SRTM.

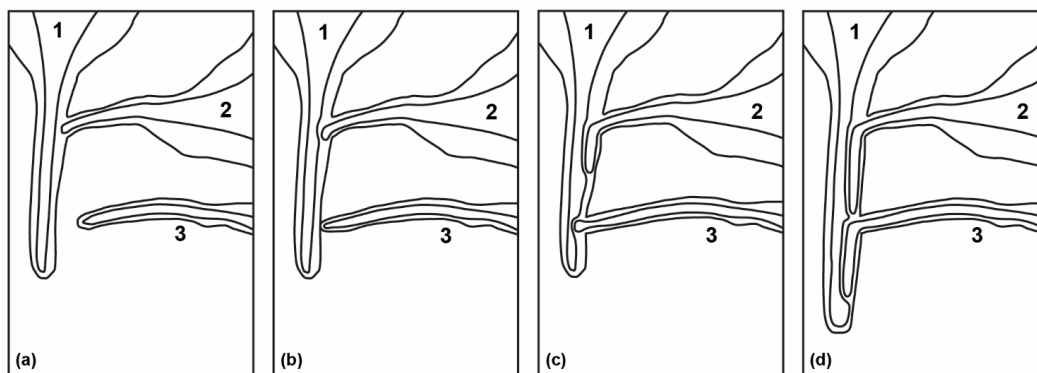
711



712

713 Fig. 4: Comparison of glacier outlines from the original inventory GI-2 (blue/white)
714 GI-3max (yellow/red) showing the minimum and maximum extents of two surging glaciers. Image source:
715 earthexplorer.usgs.gov.

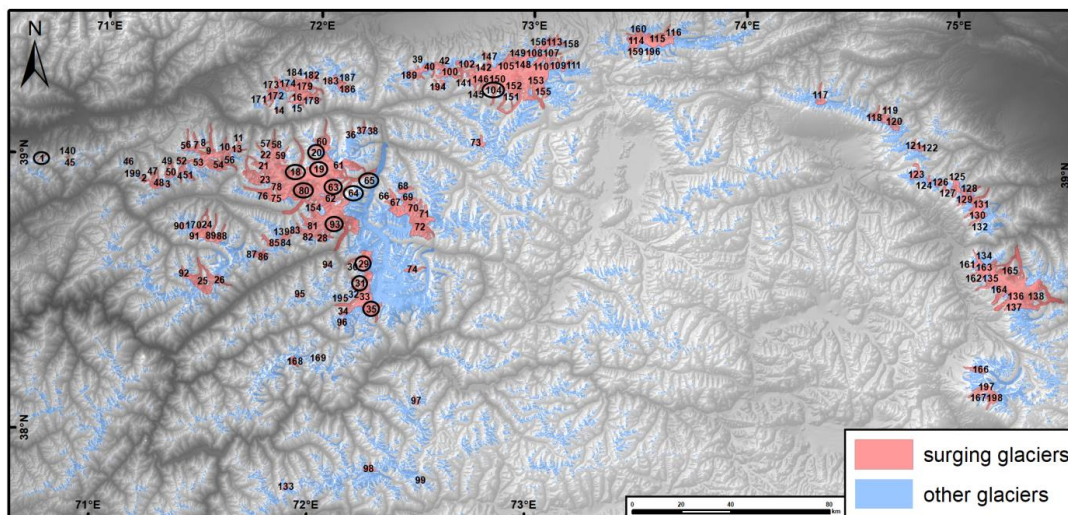
716



717

718 Fig. 5: Sketch map of selected possible interactions among surging glaciers of different types. a) At the
719 beginning, b) surge start glacier 2, c) surge start glacier 3, d) surge of glacier 1. See text for discussion.

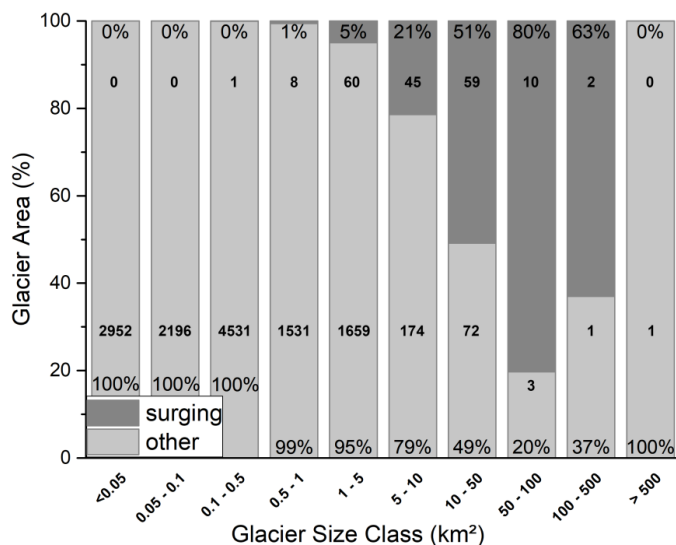
720



721

722 Fig. 6: Overview of the identified surging glaciers (red) in the Pamir Mountains. Small black numbers refer to
 723 their ObjectID in the GI-3min dataset and numbers in circles indicate glaciers mentioned in the text. DEM
 724 source: AW3D30.

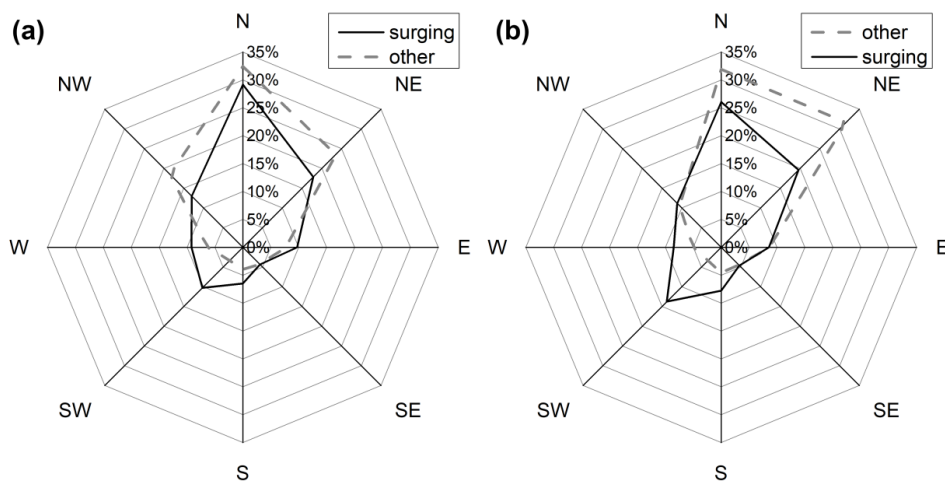
725



726

727 Fig. 7: Size class distribution (in relative terms) of surging and other glaciers in GI-2. The upper bold numbers
 728 provide the count for surge glaciers, the lower one for all other glaciers.

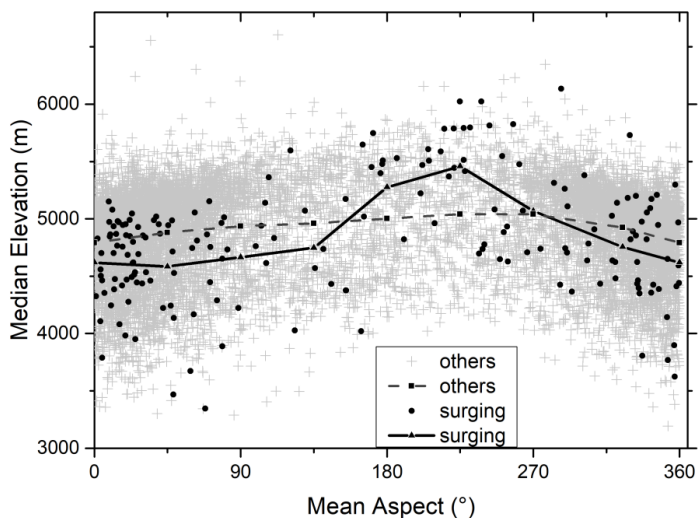
729



730

731 Fig. 8: Aspect sector distribution for surging and other glaciers (in relative terms) per a) count and b) area
732 covered.

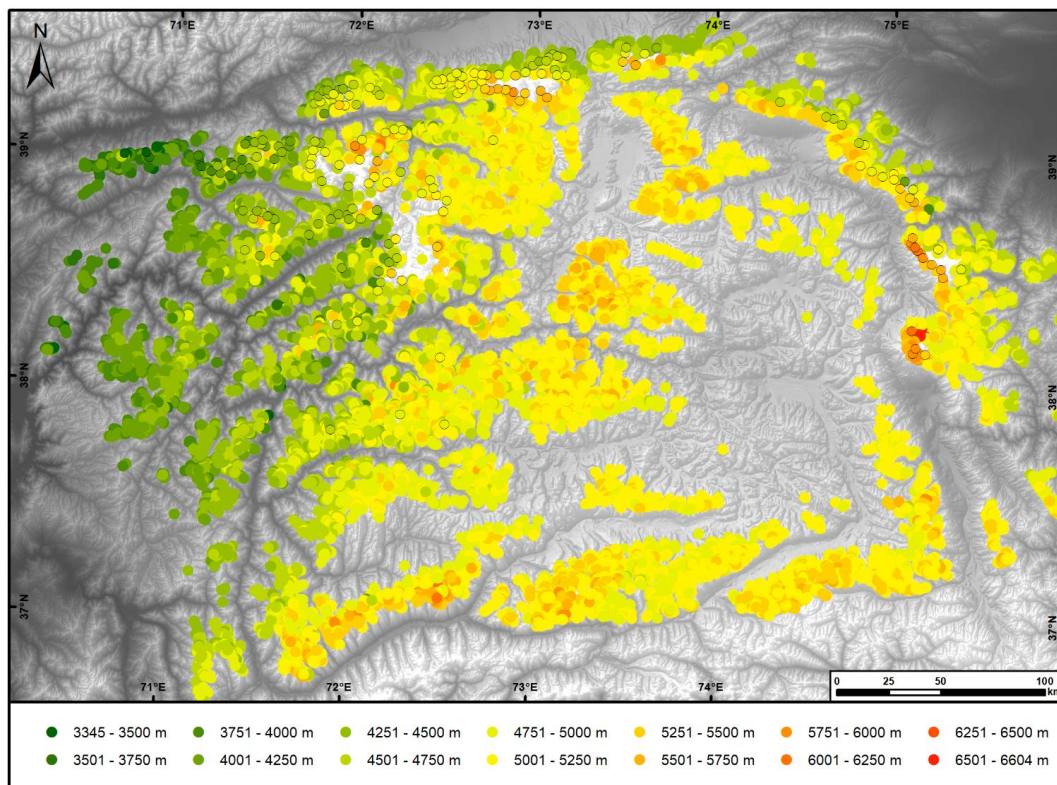
733



734

735 Fig. 9: Mean aspect vs. median glacier elevation for surging and other glaciers. The connected lines are
736 averages per aspect sector.

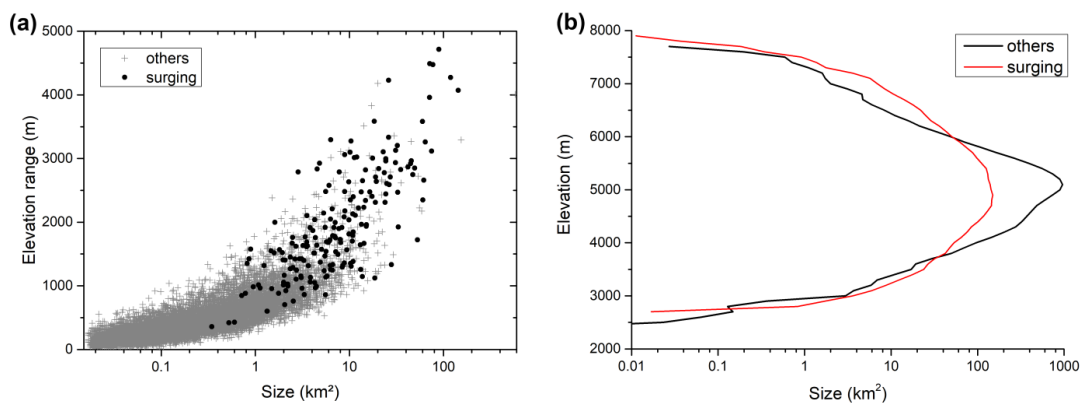
737



738

739 Fig. 10: Colour-coded median elevation map with surging glaciers marked (circles with outlines). DEM source:
 740 AW3D30.

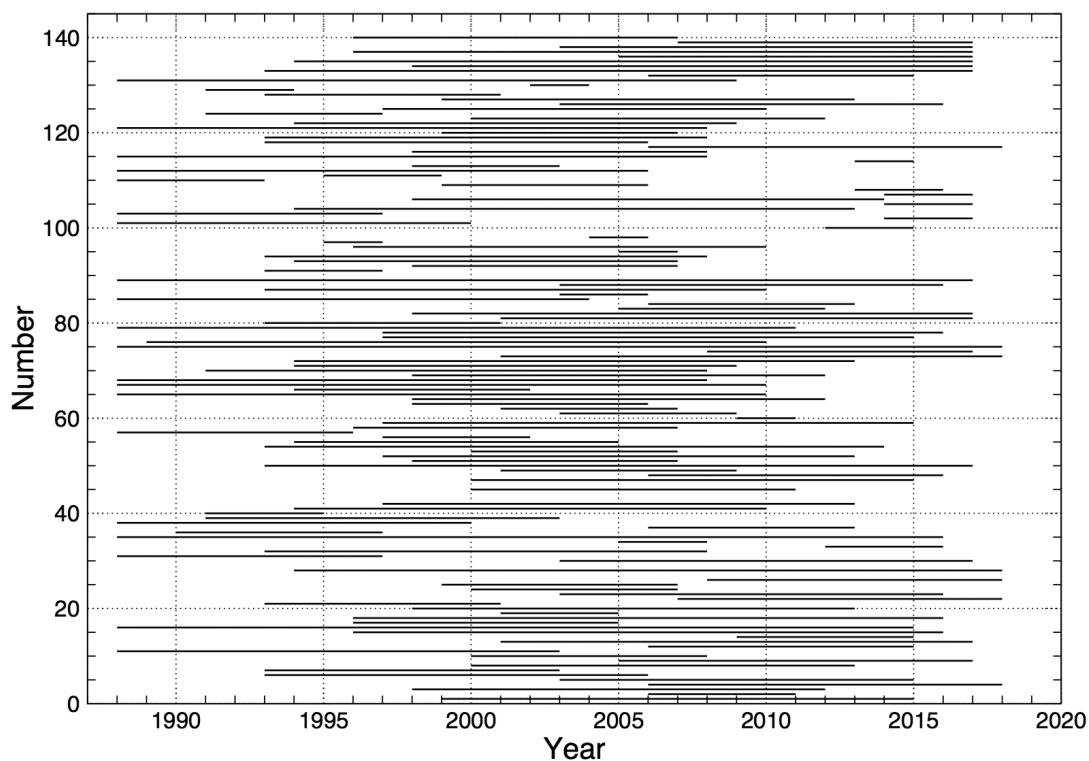
741



742

743 Fig. 11: Comparing topographic characteristics of surging glaciers to all others. a) Scatterplot of the elevation
 744 range vs. glacier size. b) Glacier hypsometry for surging and other glaciers.

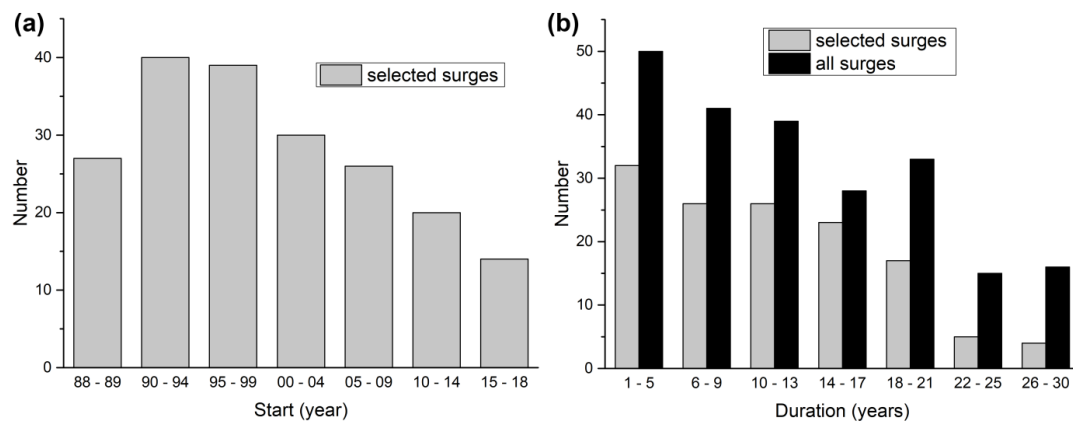
745



746

747 Fig. 12: Surge periods vs. glacier ID for all glaciers with observed surges. Those starting (ending) in 1988
 748 (2018) might have started earlier / last longer than indicated by the line.

749



750

751 Fig. 13: Histograms of surge characteristics. a) Periods in which the surges have started, b) surge durations. The
 752 charts provide greater detail than the classification code to allow for a better analysis and keep the glacier code
 753 in the inventory simple. The grey bars in b) refer to the surges that occurred completely within the study period,
 754 i.e. started after 1988 and ended before 2018.

755

756